Monopole strength function of deformed superfluid nuclei

M. Stoitsov, M. Kortelainen, T. Nakatsukasa, C. Losa, and W. Nazarewicz

Monopole strength function of deformed superfluid nuclei

M. Stoitsov,[1, 2] M. Kortelainen,[1, 2] T. Nakatsukasa,[3, 4] C. Losa,[5] and W. Nazarewicz[1, 2, 6]

[1]*Department of Physics & Astronomy, University of Tennessee, Knoxville, Tennessee 37996, USA*
[2]*Physics Division, Oak Ridge National Laboratory,*
P.O. Box 2008, Oak Ridge, Tennessee 37831, USA
[3]*RIKEN Nishina Center, Wako-shi, 351-0198, Japan*
[4]*Center for Computational Sciences, University of Tsukuba, Tsukuba, 305-8571, Japan*
[5]*International School for Advanced Studies, SISSA, Via Bonomea 265 34136 Trieste, Italy*
[6]*Institute of Theoretical Physics, Warsaw University, ul. Hoża 69, 00-681 Warsaw, Poland*

We present an efficient method for calculating strength functions using the finite amplitude method (FAM) for deformed superfluid heavy nuclei within the framework of the nuclear density functional theory. We demonstrate that FAM reproduces strength functions obtained with the fully self-consistent quasi-particle random-phase approximation (QRPA) at a fraction of computational cost. As a demonstration, we compute the isoscalar and isovector monopole strength for strongly deformed configurations in ^{100}Zr and ^{240}Pu by considering huge quasi-particle QRPA spaces. Our approach to FAM, based on Broyden's iterative procedure, opens the possibility for large-scale calculations of strength distributions in well-deformed superfluid nuclei across the nuclear landscape.

Introduction.– One of the major challenges in the many-body problem is the microscopic description of the collective motion involving hundreds of strongly interacting particles. Here, of particular interest is the response of the system to a time-dependent external field. In the nuclear case, in the small-amplitude limit of nearly harmonic oscillations about equilibrium, the phenomena of interest include the variety of vibrational modes, and characteristic distribution of electromagnetic, particle, and beta-decay strength [1, 2].

Most nuclei exhibit strong nucleonic pairing that profoundly impacts their collective motion [3, 4]. When moving away from the stability line, another factor affecting nuclear correlations, and dynamics is the presence of a low-lying particle continuum which provides a vast configuration space for nucleonic excitations. Therefore, to understand the variety of nuclear modes throughout the nuclear chart, a consistent treatment of many-body correlations and continuum is required [5].

This study is devoted to the monopole strength in superfluid deformed heavy nuclei. The theoretical method is the quasi-particle random-phase approximation (QRPA) applied to the self-consistent configuration obtained by means of the nuclear density functional theory (DFT) [6]. QRPA represents a small amplitude limit to the time-dependent superfluid DFT method. In the absence of pairing, QRPA reduces to the usual Random Phase Approximation (RPA) built atop the Hartree-Fock (HF) equilibrium.

In the electronic DFT, the RPA contribution to electron correlation energies has emerged [7, 8] as an important building block of accurate density functional treatments of molecules and solids as it combines a number of attractive features: it includes the long-range dispersion [9] as opposed to semi-local functionals; it is non-perturbative and can be applied to small or zero gap problems, such as metals [10] or dissociating H_2 [11]; it

is nearly exact in the high-density or low-coupling limit, and it is parameter-free; finally it is intimately related to the microscopic Coupled Cluster doubles theory [12–14]. In the nuclear DFT, the applicability of (Q)RPA to correlation energies is more limited [15–17] as many nuclei have transitional character, i.e., they are close to the critical point for the symmetry-breaking where the second-order expansion in density fluctuations breaks down [18]. In spite of its drawbacks, because of its deep connection to DFT, QRPA is still the tool of choice when it comes to either spherical or well-deformed nuclei. In addition to numerous applications to small-amplitude collective motion, QRPA for deformed nuclei may be utilized in the calculation of the collective mass for the large-amplitude dynamics [19].

The advantage of QRPA+DFT is that it properly takes into account self-consistent couplings giving rise to the variety of symmetry-breaking phenomena and, when done properly, includes the effects due to the continuum coupling. Due to the complexity of the problem, the QRPA framework being capable of a fully self-consistent description of non-spherical systems has eluded us until very recently [20–24].

A major obstacle preventing the widespread use of QRPA has been its high computational cost. In chemistry, this factor has limited applications of this method considerably [8]. In nuclear physics, most fully self-consistent QRPA applications have been limited to spherical nuclei (see, e.g., [25] and references therein). In spite of advanced computational resources available, it is only very recently that deformed QRPA calculations atop the Hartree-Fock-Bogoliubov (HFB) equilibrium have been carried out [20–24].

The primary challenge in the conventional matrix formulation of (Q)RPA is computation and storage of huge matrices of the residual interaction. The recent breakthrough came from the realization that both bot-

tlenecks can be avoided by taking advantage of self-consistent DFT solutions and directly employing the linear response theory to them (see literature quoted in Refs. [14, 26, 27]). Indeed, in both the finite-amplitude method (FAM) [26] and the iterative non-Hermitian Arnoldi diagonalization technique [27], the (Q)RPA matrix equations are recast into the set of self-consistent equations with respect to (Q)RPA amplitudes, which significantly reduces computational effort. The FAM has been applied in the RPA variant to Skyrme energy density functionals (EDFs) to study giant dipole resonances and low-lying pygmy dipole modes [28, 29]. Recently, in its QRPA extension, FAM was used to study monopole resonances in a spherical drip-line nucleus ^{174}Sn [30]. The iterative Arnoldi diagonalization was first used in the RPA variant to electromagnetic strength functions in ^{132}Sn [27], and the spherical QRPA extension has recently been reported [31].

While based on the same principle, the actual numerical implementations of FAM and iterative Arnoldi diagonalization differ. In the applications of FAM, the (Q)RPA amplitudes are iterated at desired energies. The Arnoldi algorithm is a Krylov subspace iterative method for extracting a *partial* eigenspectrum, i.e., it computes a discrete set of states that approximate true eigenvectors. (For another nuclear application, an iterative Lanczos-based power iteration algorithm for solving the RPA equations, see Ref. [32].) The number of states found is equal to the number of iterations, and these states (usually different from QRPA modes) are used to construct the strength function.

The current implementation of FAM has so far been done in the coordinate-space representation that requires a large number of iterations (in some cases more than 500-1,000 [26, 28]) to obtain self-consistent amplitudes. Here, we propose a fast and efficient method for solving the FAM-QRPA equations in the harmonic oscillator (HO) basis using the Broyden iterative scheme [33, 34] previously adopted to HFB equations of nuclear DFT [35]. We study the performance of the method and compare it with the standard QRPA diagonalization method. We demonstrate that FAM-QRPA solutions can be obtained with typically 40 iterations at modest memory requirements of about half a gigabyte for large model spaces corresponding to extreme cases of fission isomers in the actinides.

Finite Amplitude Method.– The basic formulation of the FAM-RPA is presented in Ref. [26], and that for the FAM-QRPA is given in Ref. [30]. The implementation of a traditional matrix formulation QRPA method (MQRPA) used in this work follows that of Ref. [21]. In this section, we recapitulate the method and define all necessary quantities.

The variation of the total DFT energy defined through an energy density $\mathcal{E}(\rho, \kappa, \kappa^*)$, with respect to the particle and pairing density matrices, $\rho = V^*V^T$ and $\kappa = V^*U^T$,

results in the HFB equations

$$\begin{pmatrix} h - \lambda & \Delta \\ -\Delta^* & -h^* + \lambda \end{pmatrix} \begin{pmatrix} U_\mu \\ V_\mu \end{pmatrix} = E_\mu \begin{pmatrix} U_\mu \\ V_\mu \end{pmatrix}, \qquad (1)$$

where

$$h_{kl}[\rho, \kappa, \kappa^*] = \frac{\partial \mathcal{E}[\rho, \kappa, \kappa^*]}{\partial \rho_{lk}}, \ \Delta_{kl}[\rho, \kappa] = \frac{\partial \mathcal{E}[\rho, \kappa, \kappa^*]}{\partial \kappa_{kl}^*}, \ (2)$$

E_μ are the quasi-particle energies, (U_μ, V_μ) are the two-component HFB quasi-particle vectors, and the chemical potential λ is introduced to conserve the average particle number.

The QRPA equations for the mode amplitudes ($X_{\mu\nu}$, $Y_{\mu\nu}$) and excitation energies ω can be written in a matrix form as:

$$\begin{pmatrix} A & B \\ B^* & A^* \end{pmatrix} \begin{pmatrix} X \\ Y \end{pmatrix} = \omega \begin{pmatrix} X \\ -Y \end{pmatrix} \qquad (3)$$

with matrices A and B coming from second variational derivatives of $\mathcal{E}[\rho, \kappa, \kappa^*]$ with respect to ρ and κ. In MQRPA, Eqs. (3) are solved by means of the explicit diagonalization, and the strength function corresponding to the one-body operator $\hat{F}$ is subsequently computed. In our results, strength functions calculated with MQRPA are smeared with a Lorentzian-averaging function having a width $\Gamma = 2\gamma$. Such an averaging can be associated with complex QRPA frequencies $\omega + i\gamma$ that are introduced in the context of strength function technique with schematic interactions [1, 36–38]. In fact, strength functions obtained in such a way do not require knowledge of individual RPA eigenvalues; the summation over the RPA spectrum is replaced by integration over energy (see also Refs. [15, 16]).

Following the earlier applications of FAM [26, 28–30], we solve the QRPA problem in the presence of a one-body external perturbation $\hat{F}$ of a given frequency ω. In this case, Eq. (3) can be rewritten in an alternative way [30]:

$$\begin{aligned} (E_\mu + E_\nu - \omega) X_{\mu\nu} + \delta H_{\mu\nu}^{20}(\omega) &= F_{\mu\nu}^{20}, \\ (E_\mu + E_\nu + \omega) Y_{\mu\nu} + \delta H_{\mu\nu}^{02}(\omega) &= F_{\mu\nu}^{02}, \end{aligned} \qquad (4)$$

where the complex antisymmetric matrices

$$\begin{aligned} \delta H^{20}(\omega) &= U^\dagger \delta h(\omega) V^* - V^\dagger \delta h(\omega)^T U^* \\ &\quad - V^\dagger \overline{\delta\Delta}^*(\omega) V^* + U^\dagger \delta\Delta(\omega) U^*, \\ \delta H^{02}(\omega) &= U^T \delta h(\omega)^T V - V^T \delta h(\omega) U \\ &\quad - V^T \delta\Delta(\omega) V + U^T \overline{\delta\Delta}(\omega)^* U, \end{aligned} \qquad (5)$$

are defined in terms of the non-Hermitian variations

$$\begin{aligned} \delta h(\omega) &= (h[\rho_\eta, \kappa_\eta, \bar{\kappa}_\eta] - h[\rho, \kappa, \kappa^*])/\eta, \\ \delta\Delta(\omega) &= (\Delta[\rho_\eta, \kappa_\eta] - \Delta[\rho, \kappa])/\eta, \\ \overline{\delta\Delta}(\omega) &= (\Delta[\bar{\rho}_\eta, \bar{\kappa}_\eta] - \Delta[\rho, \kappa])/\eta, \end{aligned} \qquad (6)$$

where η is a small parameter to numerically expand densities up to the first order. The non-Hermitian density matrices in (6) are:

$$\begin{aligned}
\rho_\eta &= \ (V + \eta U^* X^*)^* (V + \eta U^* Y)^T, \\
\kappa_\eta &= -(U + \eta V^* Y)(V + \eta U^* X^*)^\dagger, \\
\bar{\rho}_\eta &= \ (V + \eta U^* Y)^* (V + \eta U^* X^*)^T, \\
\bar{\kappa}_\eta &= -(U + \eta V^* X^*)(V + \eta U^* Y)^\dagger.
\end{aligned} \quad (7)$$

We note that the above density matrices depend on the external field $\hat{F}$ through the QRPA vectors (X, Y).

The FAM-QRPA equations (4) can be formally solved with respect to $X_{\mu\nu}$, $Y_{\mu\nu}$:

$$X_{\mu\nu} = -\frac{\delta H^{20}_{\mu\nu}(\omega) - F^{20}_{\mu\nu}}{E_\mu + E_\nu - \omega}, \quad Y_{\mu\nu} = -\frac{\delta H^{02}_{\mu\nu}(\omega) - F^{02}_{\mu\nu}}{E_\mu + E_\nu + \omega}. \ (8)$$

Since the matrices $\delta H^{20}(\omega)$ and $\delta H^{02}(\omega)$ linearly depend on $X_{\mu\nu}$ and $Y_{\mu\nu}$, a self-consistent iterative scheme needs to be adopted to find the QRPA amplitudes. In essence, FAM replaces the calculation and diagonalization of the large QRPA matrices A, B with a much simpler procedure of calculating $\delta H^{20}(\omega)$ and $\delta H^{02}(\omega)$, and solving Eqs. (4) at desired values of ω. To guarantee that the FAM-QRPA solution carries a finite strength function for every value of ω, we take $\omega \to \omega + i\gamma$ with a small imaginary part γ. As we shall see later, such a choice corresponds to a Lorentzian smearing of $\Gamma = 2\gamma$, except for the vicinity of $\omega = 0$ [1]. It is worth noting that the FAM implementation of QRPA is straightforward and EDF-independent, as the same HFB procedures that define the fields h, Δ in terms of particle and pairing densities are also used in FAM-QRPA calculations.

Ideally, a self-consistent iterative FAM-QRPA procedure should converge rapidly and the result should not depend on η if its value is small enough. In practice, a direct iteration of (8) diverges in most cases, especially when γ is small and/or when ω is close to the true QRPA root. Indeed, when $\gamma \to 0$, the left-hand side of Eqs. (4) becomes singular; hence, instabilities are expected around QRPA roots. To guarantee numerical stability, one has to resort to a procedure which 'mixes' the solutions from previous and next iterations. To this end, the conjugate gradient method and its derivatives were utilized in coordinate-space applications [26, 28–30]. In this work, based on the HO expansion technique, the modified Broyden's procedure [34, 35] has been adopted and turned out to yield stable results while providing excellent computational performance. For a system of linear equations (4), Broyden iterations exhibit the Q-superlinear convergence [39].

Results.– To benchmark FAM-QRPA for deformed nuclei and check its performance, we carried out FAM and MQRPA [21] calculations using the SLy4 EDF [40] and a contact volume pairing with a 60 MeV cutoff with respect to the reference single-particle energies [41]. To facilitate comparison with MQRPA implementation of Ref. [21], the center-of-mass correction has been ignored in this test. The pairing strength was chosen to reproduce the experimental neutron pairing gap of ^{120}Sn. All HFB calculations were performed with the DFT code HFBTHO [41] that solves the Skyrme-HFB equations in the HO (or transformed HO, THO) basis, assuming axial and reflection symmetries.

As discussed in Ref. [21], MQRPA calculations are subject to two truncations. The first truncation pertains to the maximum rank of the QRPA Hamiltonian matrix. To this end, one neglects all canonical states with single-particle energies greater than some cutoff value. The second truncation is made by excluding those QRPA quasiparticle pairs that have occupation probabilities less than some small critical value v^2_{crit} or larger than $1 - v^2_{\mathrm{crit}}$.

The benchmarking calculations have been carried out for the monopole isoscalar (IS) and modified isovector (IV) response operators:

$$f^{IS} = \frac{eZ}{A} \sum_{i=1}^{A} r_i^2, \quad f^{IV} = \frac{eZ}{A} \sum_{i=1}^{N} r_i^2 - \frac{eN}{A} \sum_{i=1}^{Z} r_i^2. \ (9)$$

This choice makes coupling between IS and IV monopole vibrations small [42]. At each value ω, the imaginary part has been set to $\gamma = 0.5$ MeV, and the FAM strength function has been calculated according to [30]

$$S(f, \omega) = -\frac{1}{\pi\alpha} \mathrm{Im\ Tr} \left[f(UXV^T + V^*Y^TU^\dagger) \right]. \ (10)$$

Here, the external field in Eq. (4) is given by $F = \alpha f$, where α is a parameter with dimension $[\alpha] = [F][f]^{-1}$. Since for very small values of η the QRPA amplitudes X and Y are proportional to α, $S(f, \omega)$ is independent of α. Using a complex frequency $\omega + i\gamma$, the resulting $S(f, \omega)$ possesses the crossing symmetry $S(f, \omega) = -S(f, -\omega)$ [1]; hence $S(f, \omega = 0) = 0$ is guaranteed. The strength function obtained in MQRPA has been computed by averaging QRPA diagonalization results with $\Gamma = 2\gamma = 1$ MeV. In the fully self-consistent framework, the MQRPA and FAM-QRPA results should be identical.

The MQRPA and FAM-QRPA $J^\pi = 0^+$ strength functions are compared in Fig. 1 for an oblate minimum in ^{24}Mg. (In the prolate ground state of this nucleus, paring correlations vanish.) To include the whole available space of canonical wave functions in MQRPA, the results shown in Fig. 1 were obtained using a relatively small single-particle basis corresponding to $N_{\mathrm{sh}} = 5$ HO shells. It is clearly seen that both methods yield practically identical results. Increasing the number of basis states rapidly increases the scale of the MQRPA scheme. For example, with 20 HO shells and $v_{\mathrm{crit}} = 10^{-4}$, QRPA matrices reach dimension 32,039, requiring 16.4 GB memory. Lowering the canonical cutoff to $v_{\mathrm{crit}} = 10^{-20}$ results in the matrix rank 211,159, or 713.41 GB of memory. In contrast, the memory required by FAM-QRPA, using the full space of 20 HO shells and without any truncations on a QRPA level, is a modest 0.572 GB.

The accuracy of any QRPA implementation can be assessed by its ability to handle the spurious (zero-energy) modes. In general, QRPA solutions should
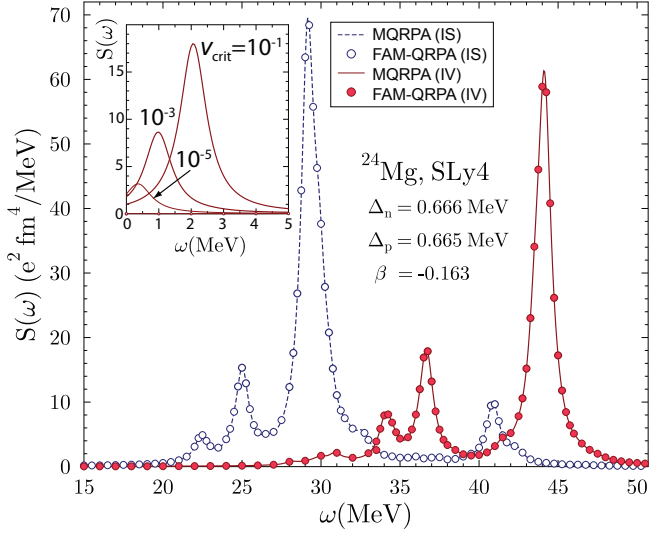
FIG. 1: (color online) The isoscalar (blue, dashed line) and isovector (red, solid line) monopole strength function in oblate-deformed and paired minimum of ^{24}Mg obtained in MQRPA within the full $N_{\rm sh} = 5$ HO space ($v_{\rm crit}$=0) and FAM-QRPA (circles). The inset shows the presence of 0^+ spurious mode at low-energy at three different values of $v_{\rm crit}$ in MQRPA.
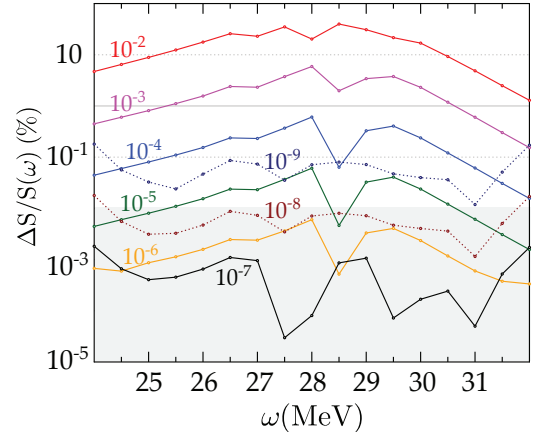

FIG. 2: (color online) The performance of the FAM-QRPA algorithm applied to the case of Fig. 1 for different values of η in the frequency range of $24<\omega<32$ MeV. The relative accuracy is defined as $\Delta S/S$ where $\Delta S(\eta) = |S(10\eta) - S(\eta)|$.
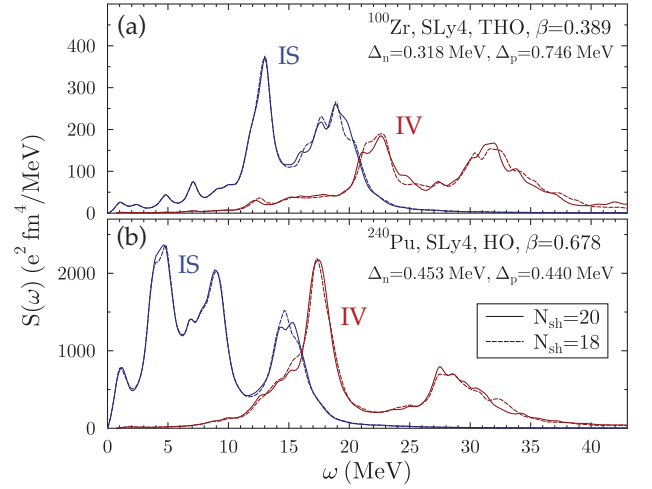

FIG. 3: (color online) IS and IV monopole strength in the deformed ground state of ^{100}Zr (top) and the superdeformed fission isomer ^{240}Pu (bottom) in FAM-QRPA with $N_{\rm sh}$=18 (dashed line) and 20 (solid line).

be properly orthogonalized against spurious modes by means of a well-established procedure [26, 27]. For the monopole case presented in Fig. 1, the configuration space of FAM-QRPA seems to be sufficient to remove the 0^+ spurious modes associated with particle-number breaking almost exactly. This is indeed seen in the inset of Fig. 1 which displays the low-energy IV monopole strength in MQRPA for several values of $v_{\rm crit}$. The MQRPA response corresponding to $v_{\rm crit}$=0 (full HO space) shows the single low-energy peak carrying the strength of about $2 \cdot 10^{-6}\, e^2{\rm fm}^4/$MeV, and the low-energy FAM-QRPA strength is of similar magnitude.

Figure 2 demonstrates that the FAM results practically do not depend on the choice of the parameter η entering the numerical derivatives in Eq. (6) for quite a large range of values of η from 10^{-6} to 10^{-8}. For $\eta < 10^{-8}$ numerical noise starts to deteriorate the accuracy of the calculation. Usually, the FAM solution is reached fairly quickly, within 10-50 iterations assuming that the maximum difference between collective amplitudes in two consecutive iterations is less that 10^{-6}.

In order to demonstrate the ability of FAM-QRPA to treat heavy, deformed, and superfluid nuclei, Fig. 3 shows the monopole strength distributions for the ground state of ^{100}Zr (previously studied in [43]) and fission isomer in ^{240}Pu. For the neutron-rich nucleus ^{100}Zr, calculations were carried out in large configuration spaces of $N_{\rm sh} = 18$ and 20 of the stretched THO [41]. For the superdeformed state of ^{240}Pu, we took the stretched HO basis with $N_{\rm sh} = 18$ and 20. As demonstrated in Fig. 3, by taking $N_{\rm sh} = 20$, the computed monopole strength is

practically stable in the whole range of ω in the both cases considered. As it is well known [44], due to its large deformation, the IS monopole strength distribution splits into two components. Here, as well as in other cases considered in this work, about 99% of the EWSR is exhausted when integrating up to ω=50 MeV. For ^{100}Zr, the calculated strength distribution nicely agrees with that of Ref. [43]. Both examples nicely illustrate the applicability of FAM-QRPA to the local QRPA approach used in the context of the large-amplitude collective motion [19].

Conclusions.– In this work we applied the FAM-QRPA method to describe the multipole strength in deformed and superfluid nuclei. A new efficient method for the iterative solution of FAM-QRPA equations, based on the Broyden mixing procedure [35], has been proposed. The

algorithm is especially suited for multiprocessor tasks since the QRPA strength distribution $S(\omega)$ converges with typically 40 iterations regardless of ω.

The calculations have been presented for IS and IV monopole modes. We first benchmarked FAM-QRPA against the MQRPA approach of Ref. [21] and obtained excellent agreement. As compared to the standard diagonalization method, FAM-QRPA offers excellent performance, both in terms of memory and speed. Including all the fields (both time-even and time-odd) required by the fully self-consistent QRPA, the memory requirement for the FAM-QRPA module built on the top of the DFT solver HFBTHO does not exceed 572 MB. This enables us to handle axially-deformed heavy nuclei without imposing any truncation on the QRPA level. The self-consistency of FAM-QRPA, together with very large pairing windows employed, results in a practical decoupling of the 0^+ spurious modes associated with the particle-number symmetry breaking. The illustrative examples have been presented for strongly deformed configurations in ^{100}Zr and ^{240}Pu. It has been demonstrated that the convergent result are obtained by taking a large basis of 20 HO (or THO) shells.

The proposed FAM implementation allows fast calculations of monopole strength for all axially deformed nuclei throughout the nuclear chart. The implementation of the method to higher multipolarity modes is straightforward, and is in progress. Another future development is the extension of the method to very weakly bound systems. Here, the precise description of the low-energy non-resonant continuum will require the departure from the currently employed HO (or THO) basis by using the Gamow HFB approach [45].

[1] A. Bohr and B.R. Mottelson, *Nuclear Structure*, Vol. I (W.A. Benjamin, New York, 1969); Vol. II (W.A. Benjamin, New York, 1975).

[2] P. Ring and P. Schuck, *The Nuclear Many-Body Problem* (Springer Verlag, New York, 1980).

[3] D. Rowe, *Nuclear Collective Motion, Models and Theory* (Mathuen, London, 1970).

[4] D.M. Brink and R.A. Broglia, *Nuclear Superfluidity: Pairing In Finite Systems* (Cambridge Univ. Press, Cambridge, 2005).

[5] J. Dobaczewski *et al.*, Prog. Part. Nucl. Phys. **59**, 432 (2007).

[6] M. Bender, P.-H. Heenen, and P.-G. Reinhard, Rev. Mod. Phys. **75**, 121 (2003).

[7] D. C. Langreth and J.P. Perdew, Phys. Rev. B **15**, 2884 (1977).

[8] F. Furche, J. Chem. Phys. **129**, 114105 (2008).

[9] J. Dobson, in *Time-Dependent Density Functional Theory*, Vol. 706, p 443 (Springer, Berlin Heidelberg, 2006).

[10] J. Harl and G. Kresse, Phys. Rev. B **77**, 045136 (2008); Phys. Rev. Lett., **103**, 056401 (2009).

[11] F. Weigend *et al.*, Chem. Phys. Lett., **294**, 143 (1998); M. Fuchs *et al.*, Chem. Phys., **122**, 094116 (2005).

[12] D.L. Freeman and M.J. Karplus, Chem. Phys. **64**, 2641 (1976).

[13] G.E. Scuseria, T.M. Henderson, and D.C. Sorensen, J. Chem. Phys. **129**, 231101 (2008).

[14] S. Tretiak *et al.*, J. Chem. Phys. **130**, 054111 (2009).

[15] F. Dönau, D. Almehed, and R.G. Nazmitdinov, Phys. Rev. Lett. **83**, 280 (1999).

[16] Y.R. Shimizu, P. Donati, and R.A. Broglia, Phys. Rev. Lett. **85**, 2260 (2000).

[17] K. Hagino and G.F. Bertsch, Nucl. Phys. **A679**, 163 (2000).

[18] W. Nazarewicz, Nucl. Phys. **A557**, 489c (1993).

[19] N. Hinohara *et al.*, Phys. Rev. C **82**, 064313 (2010).

[20] J. Terasaki and J. Engel, Phys. Rev. C **82**, 034326 (2010).

[21] C. Losa *et al.*, Phys. Rev. C **81**, 064307 (2010).

[22] J. Terasaki and J. Engel, arXiv:1105.3817v1 (2011).

[23] S. Péru *et al.*, Phys. Rev. C **83**, 014314 (2011).

[24] M. Martini, S. Péru, and M. Dupuis, arXiv:1103.1553v1 (2011).

[25] J. Terasaki *et al.*, Phys. Rev. C **71**, 034310 (2005).

[26] T. Nakatsukasa, T. Inakura, and K. Yabana, Phys. Rev. C **76** 024318 (2007).

[27] J. Toivanen *et al.*, Phys. Rev. C **81**, 034312 (2010).

[28] T. Inakura, T. Nakatsukasa, and K. Yabana, Phys. Rev. C **80** 044301 (2009).

[29] T. Inakura, T. Nakatsukasa, and K. Yabana, arXiv:1106.3618 (2011).

[30] P. Avogadro and T. Nakatsukasa, Phys. Rev. C in press; arXiv:1104.3692.

[31] J. Toivanen *et al.*, presented at the ARIS-2011 Conference, Leuven, Belgium; to be published.

[32] C.W. Johnson, G.F. Bertsch, and W.D. Hazelton, Comput. Phys. Commun. **120**, 155 (1999).

[33] C.G. Broyden, Math. Comput. **19**, 577 (1965).

[34] D.D. Johnson, Phys. Rev. B **38**, 12807 (1988).

[35] A. Baran *et al.*, Phys. Rev. C **78**, 014318 (2008).

[36] L. A. Malov and V. G. Soloviev, Nucl. Phys. **A270**, 87 (1976).

[37] L. A. Malov, V. O. Nestorenko, and V. G. Soloviev, Theor. Math. Phys. **32**, 646 (1977).

[38] J. Kvasil *et al.*, Phys. Rev. C **58**, 209 (1998).

[39] C. T. Kelley, *SIAM Frontiers in Applied Mathematics*, SIAM, Philadelphia, 1995, no. 16.

[40] E. Chabanat *et al.*, Nucl. Phys. **A635**, 231 (1998).

[41] M.V. Stoitsov *et al.*, Comput. Phys. Commun. **167**, 43 (2005).

[42] E. Lipparini and S. Stringari, Phys. Rep. **175**, 103 (1989).

[43] K. Yoshida, Phys. Rev. C **82**, 034324 (2010).

[44] U. Garg *et al.*, Phys. Rev. Lett. **45**, 1670 (1980).

[45] N. Michel, K.Matsuyanagi, and M. Stoitsov, Phys. Rev. C **78**, 044319 (2008).